Electronic Supplementary Material (ESI) for Inorganic Chemistry Frontiers.

Construction of In_2S_3@ZIF-8@$ZnIn_2S_4$ Hierarchical Nanoflower Heterostructure to Promote Photocatalytic Reduction Activities

*Chengyuan Yang, Rong Wang, Wenxin Zhu, Jing Wang, Liang Zhang, Ting Du, Zhaoli Liu, Linxuan Xie, Jing Sun and Jianlong Wang**

[a] College of Food Science and Engineering, Northwest A&F University, Yangling, 712100, Shaanxi, P. R. China.

[b] Qinghai Key Laboratory of Qinghai-Tibet Plateau Biological Reources, Northwest Institute of Plateau Biology, Chinese Academy of Sciences, Qinghai, 810008,

Electronic Supplementary Information Index

1. Experimental Section

1.1 Materials

1.2 Materials characterization

2. Figures and Tables

Figure S1. FESEM image of In_2S_3@$ZnIn_2S_4$.

Figure S2. TEM image of In_2S_3@$ZnIn_2S_4$.

Figure S3. Elemental mappings of In_2S_3@ZIF-8@$ZnIn_2S_4$ nanoflowers.

Figure S4. HRTEM images of In_2S_3@ZIF-8@$ZnIn_2S_4$.

Figure S5. N_2 adsorption-desorption curves for In_2S_3@$ZnIn_2S_4$ and In_2S_3@ZIF-8@$ZnIn_2S_4$.

Figure S6. TGA curves for In_2S_3@$ZnIn_2S_4$ and In_2S_3@ZIF-8@$ZnIn_2S_4$.

Figure S7. Diagrammatic sketch of the e^- and h^+ transfer process for a) In_2S_3@$ZnIn_2S_4$ and b) In_2S_3@ZIF-8@$ZnIn_2S_4$.

Figure S8. Steady-state PL spectra for In_2S_3, In_2S_3@ZIF-8, In_2S_3@$ZnIn_2S_4$ and In_2S_3@ZIF-8@$ZnIn_2S_4$.

Figure S9. ESR spectra of DMPO-trapped $\cdot O^{2-}$ and $\cdot OH$ using In_2S_3@$ZnIn_2S_4$ samples subjected to 4 and 8 min visible light irradiation.

Figure S10. ESR spectra of DMPO-trapped $\cdot O^{2-}$ and $\cdot OH$ using In_2S_3@ZIF-8@$ZnIn_2S_4$ samples subjected to 4 and 8 min visible light irradiation.

Table S1 Data comparison of photocatalytic Cr(VI) reduction performance over different catalysts.

3. References

1. Experimental section

1.1 Materials

Indium nitrate hydrate ($In(NO_3)_3 \cdot xH_2O$), Zinc nitrate hexahydrate ($Zn(NO_3)_2 \cdot 6H_2O$) Zinc chloride ($ZnCl_2$), p-Phthalic acid ($C_8H_6O_4$, PTA), Polyvinylpyrrolidone (PVP), Thiourea (CH_4N_2S), thioacetamide (C_2H_5NS, TAA), 2-methylimidazole (2-MIM), N,N-Dimethylformamide (DMF) and ethanol (C_2H_5OH) were all supplied by Aladdin Industrial cooperation, Shanghai, China. All the materials were analytical grade for synthesis and used as received without further purification. Deionized water was used throughout this work from local sources.

1.2 Materials characterization

The morphology and structure of the samples were examined by scanning electron microscope (SEM) and transmission electron microscope (TEM). The SEM figures were characterized by a field emission scanning electron microscopy (FE-SEM, JSM-7001F, Japan). The compositions of the samples were analyzed by energy-dispersive X-ray spectroscope (EDX) attached to the SEM instrument. Elemental mapping images were recorded using EDX spectroscope attached to TEM (JEOL, JEM-2100F). The TEM, high-resolution transmission electron microscopy (HR-TEM) images and corresponding selected area electron diffraction (SAED) pattern were examined by transmission electron microscopy (JEM-2010, Japan). The crystal structure of the samples was analyzed by the powder X-ray diffraction (XRD model MAC Science, Japan) with Ni-filtrated Cu-Kα radiation. The scan range of 2θ was 5-80° at a scan rate of 5° min^{-1}. The X-ray photoelectron spectroscopy (XPS) measurements were measured on a PerkinElmer PHI 5300 instrument with a monochromatic Mg Kα source to test the elements on the surface of nanomaterials and the C1s signal was set to the position of 284.6 eV. UV-vis diffuse reflectance spectra (DRS) were obtained using a Varian Cary 500 UV vis-NIR spectrometer equipped with an integrating sphere. Photoluminescence (PL) spectra for solid samples were acquired on Edinburgh Analytical Instruments FL/FSTCSPC920 coupled with a time-correlated single-photo-counting system at room temperature. The transient photocurrent and electrochemical impedance spectroscopy of the as-prepared samples was obtained via an electrochemical workstation (CHI660E) under Xe lamp irradiation (300 W, $\lambda > 400$ nm) using a standard three-electrode system. The Ag/AgCl (saturated KCl) and Pt wire were utilized as the reference and counter electrodes, respectively. Meanwhile, 0.1 M Na_2SO_4 solution and a mixture of 5 mM $K_3Fe(CN)_6/K_4Fe(CN)_6$ containing 0.1 M KCl were used as the electrolyte in the transient photocurrent responses and electrochemical impedance spectroscopy (EIS) experiments, respectively.

2. Figures and Tables

Detail information of $In_2S_3@ZnIn_2S_4$:

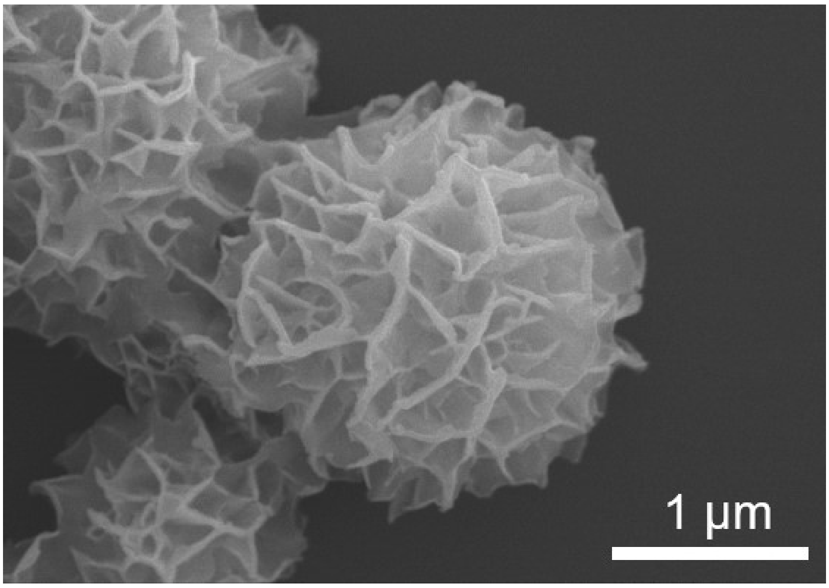

Figure S1. FESEM image of $In_2S_3@ZnIn_2S_4$.

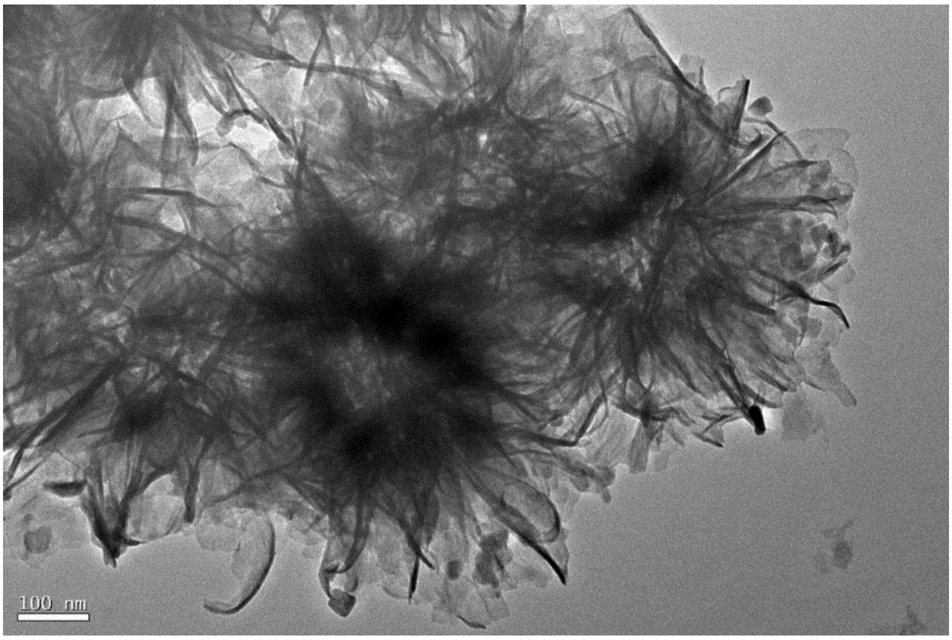

Figure S2. TEM image of In_2S_3@$ZnIn_2S_4$.

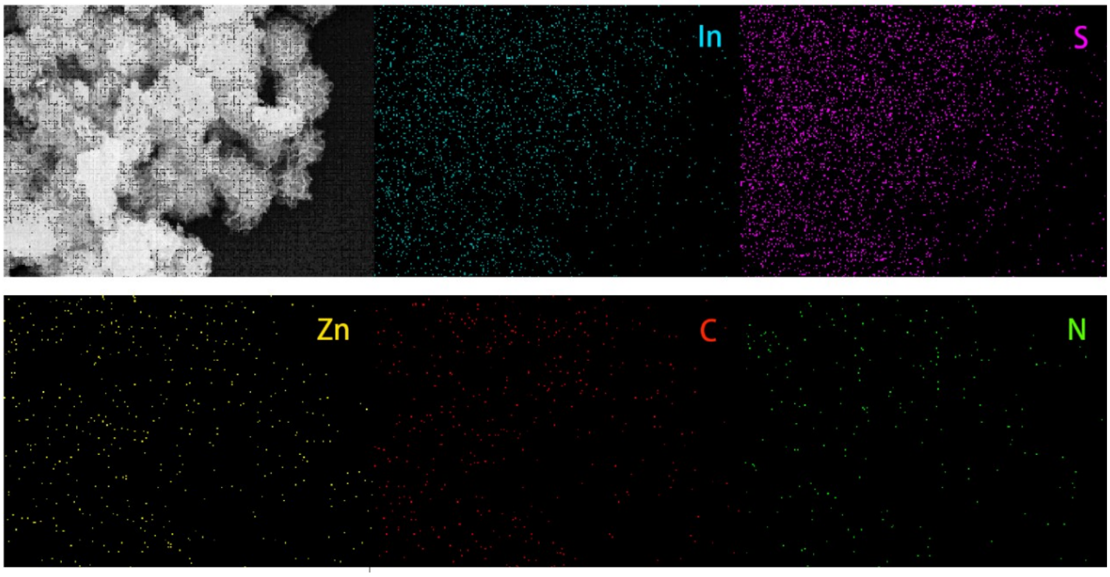

Figure S3. Elemental mappings of In_2S_3@ZIF-8@$ZnIn_2S_4$ nanoflowers.

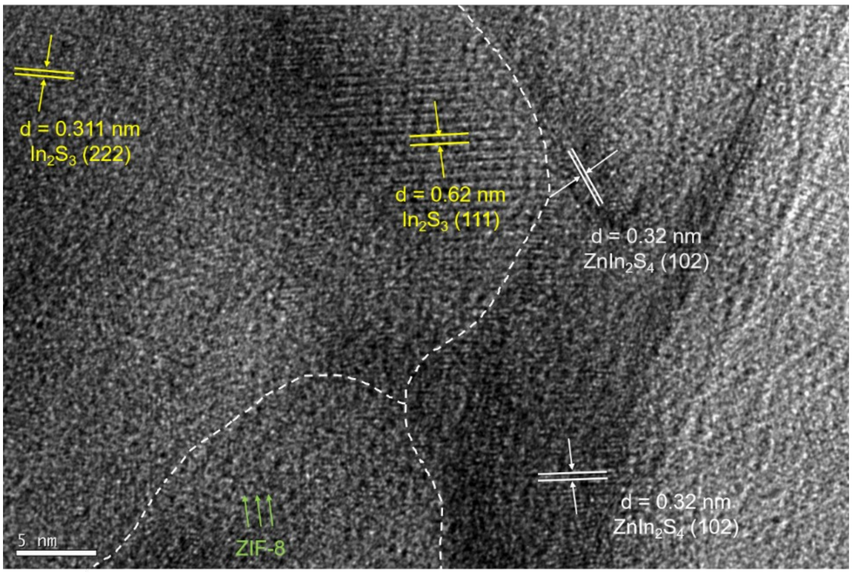

Figure S4. HRTEM images of In_2S_3@ZIF-8@$ZnIn_2S_4$.

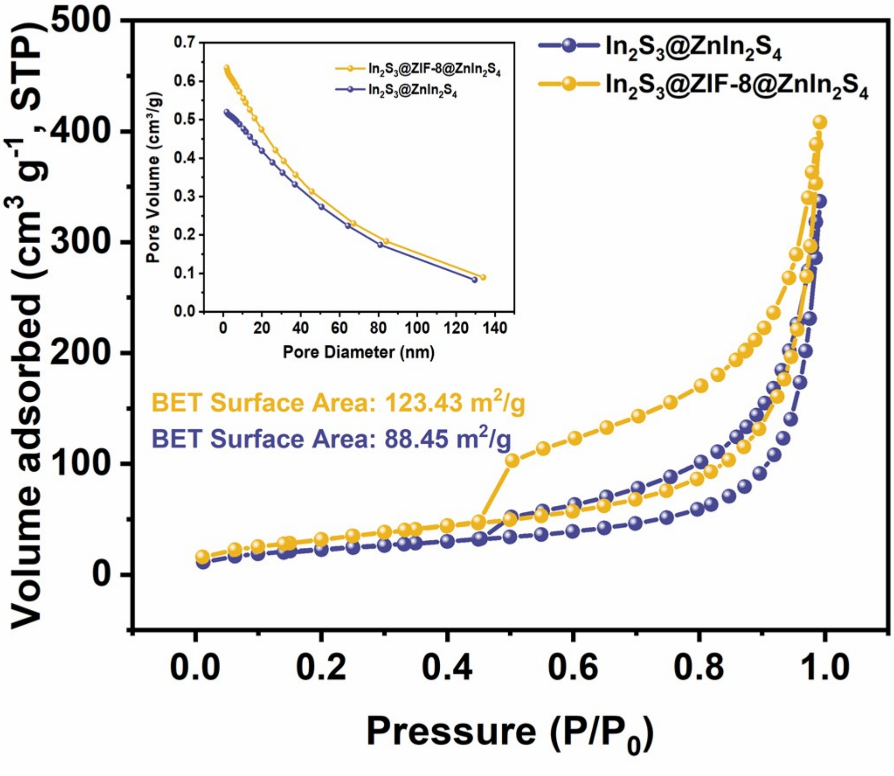

Figure S5. N_2 adsorption-desorption curves and pore size distributions for In_2S_3@$ZnIn_2S_4$ and In_2S_3@ZIF-8@$ZnIn_2S_4$.

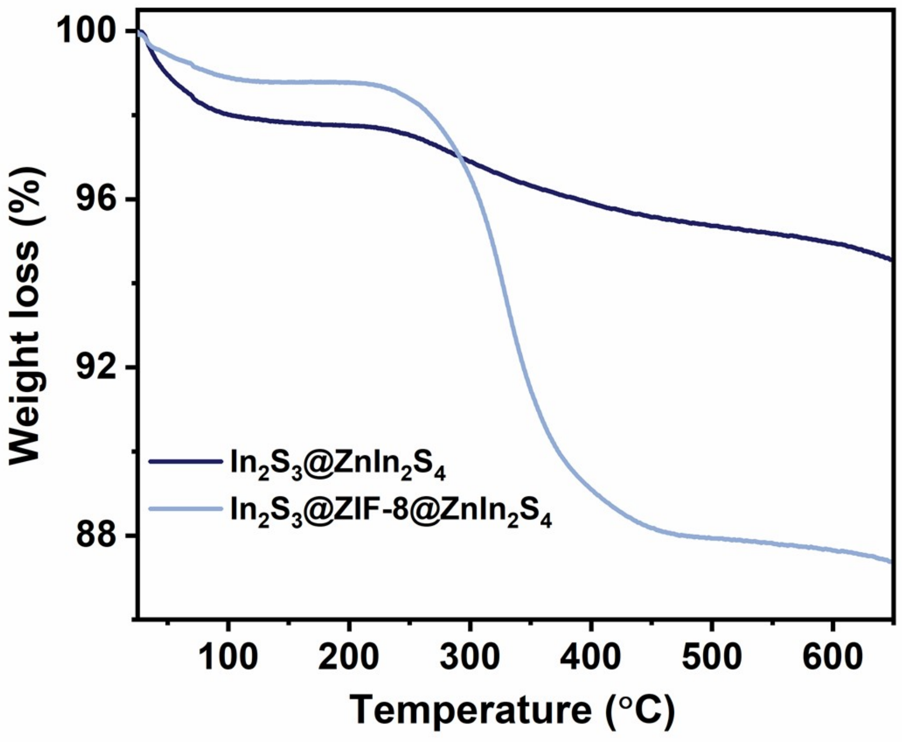

Figure S6. TGA curves for In_2S_3@$ZnIn_2S_4$ and In_2S_3@ZIF-8@$ZnIn_2S_4$.

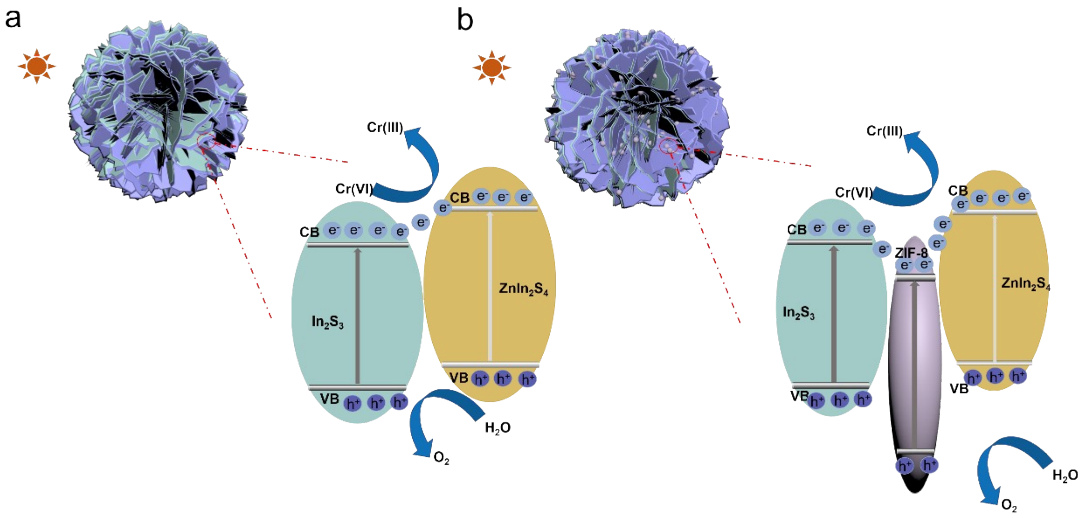

Figure S7. Diagrammatic sketch of the e^- and h^+ transfer process for a) In_2S_3@$ZnIn_2S_4$ and b) In_2S_3@ZIF-8@$ZnIn_2S_4$.

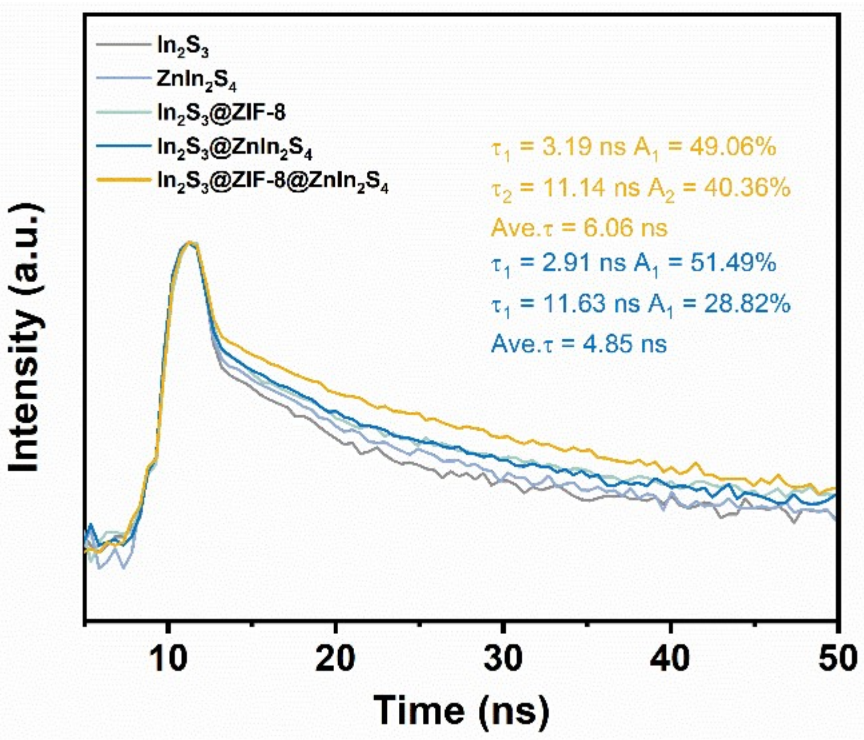

Figure S8. The local enlarged figure of average photoluminescence (PL) lifetime between In_2S_3@$ZnIn_2S_4$ and In_2S_3@ZIF-8@$ZnIn_2S_4$.

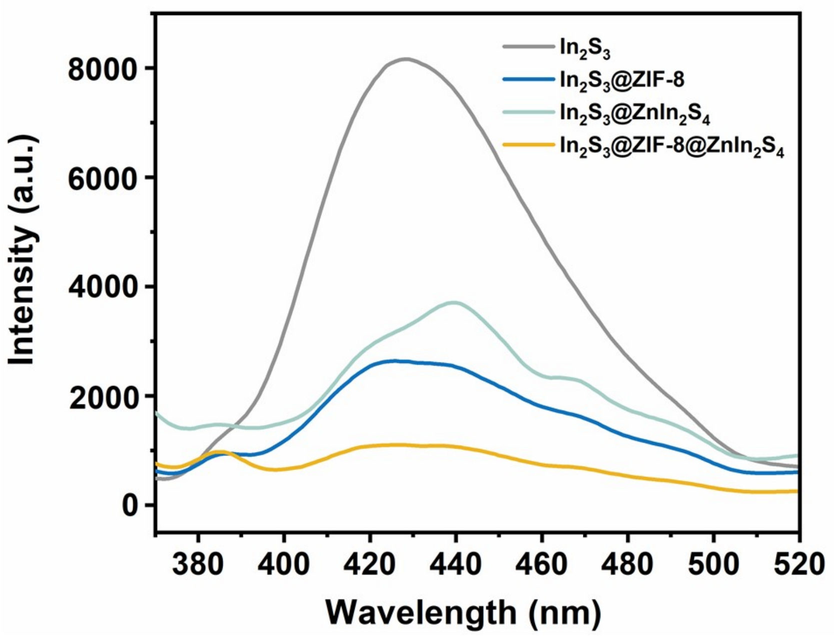

Figure S9. Steady-state PL spectra for In_2S_3, In_2S_3@ZIF-8, In_2S_3@$ZnIn_2S_4$ and In_2S_3@ZIF-8@$ZnIn_2S_4$.

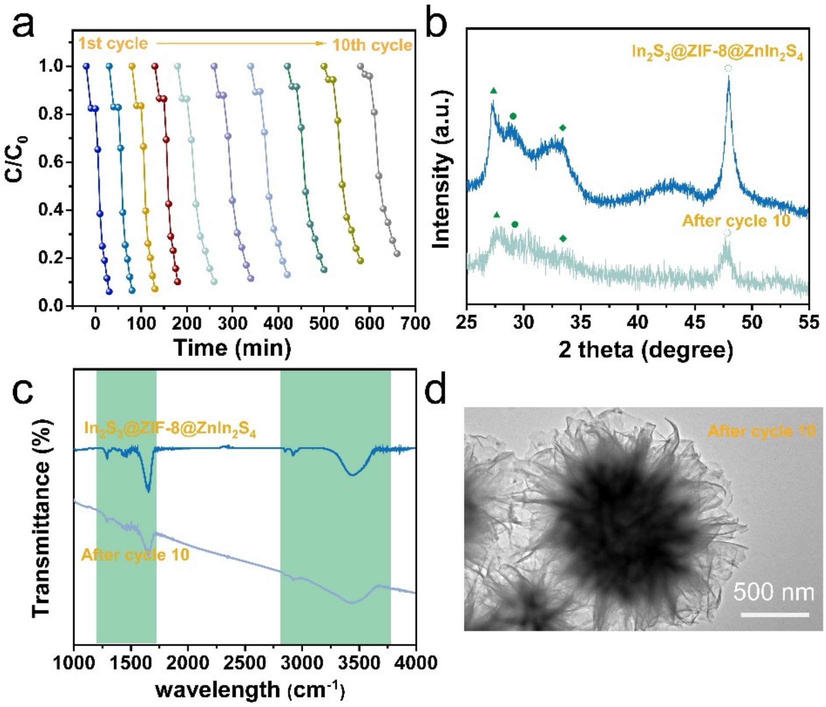

Figure S10. (a) Cycling experiments for the photocatalytic degradation of Cr(VI) by the In_2S_3@ZIF-8@$ZnIn_2S_4$; (b) XRD patterns; (c) FTIR and (d) TEM spectra of In_2S_3@ZIF-8@$ZnIn_2S_4$ before and after photocatalytic cycling ten times.

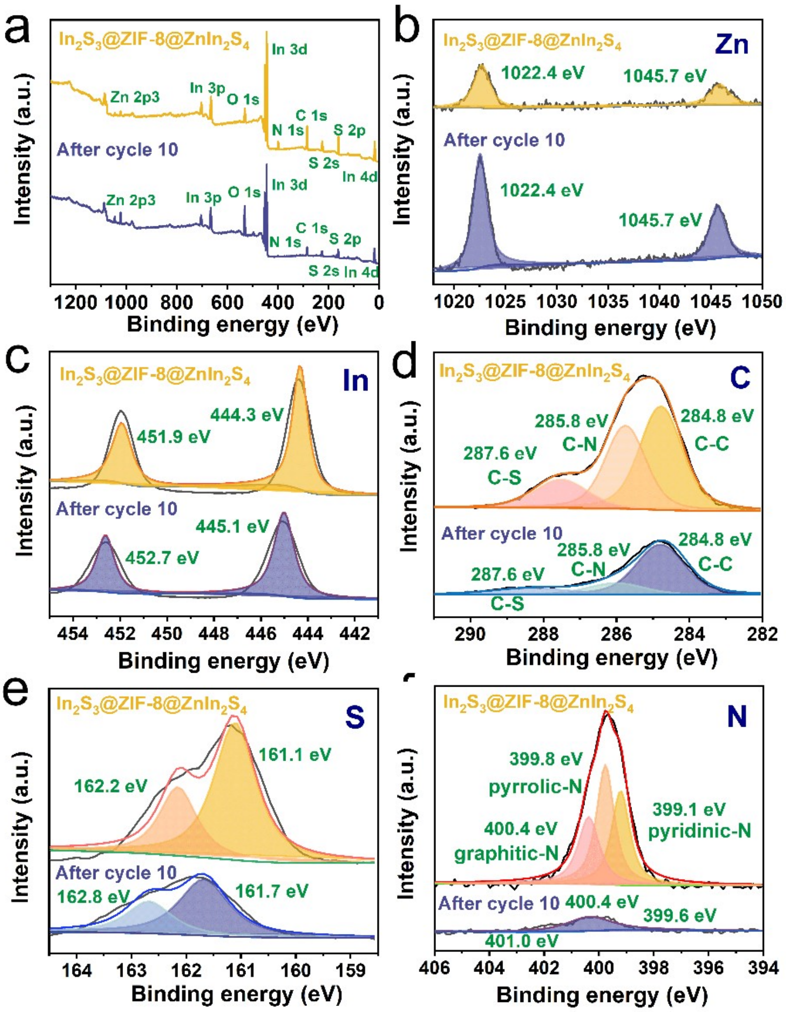

Figure S11. XPS data from the surface of the sample: (a) the whole-range spectrum of In_2S_3@ZIF-8@$ZnIn_2S_4$ before and after photocatalytic cycling ten times; (b) Zn 2p core-level spectrum; (c) In 3d core-level spectrum; (d) C 1s core-level spectrum (e) S 2p core-level spectrum; (f) N 2p of core-level spectrum.

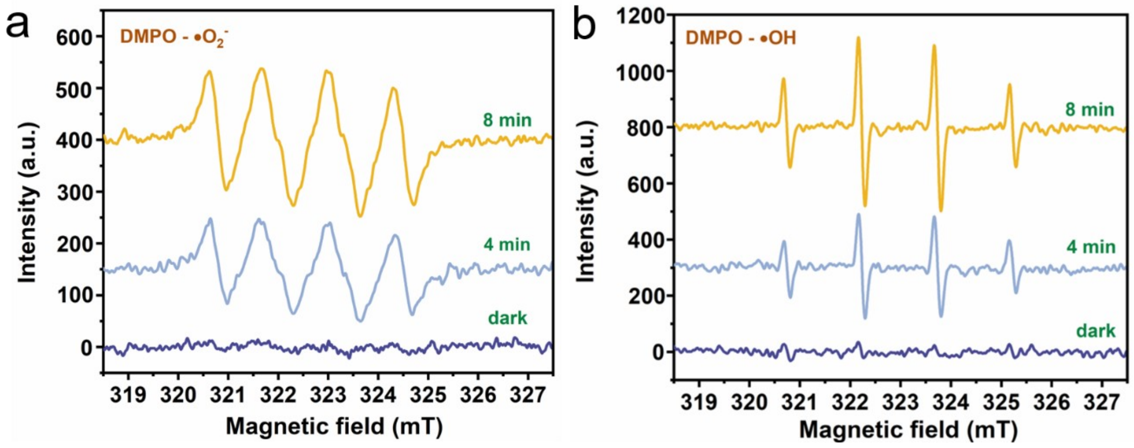

Figure S12. ESR spectra of DMPO-trapped ·O^{2-} and ·OH using In_2S_3@$ZnIn_2S_4$ samples subjected to 4 and 8 min visible light irradiation.

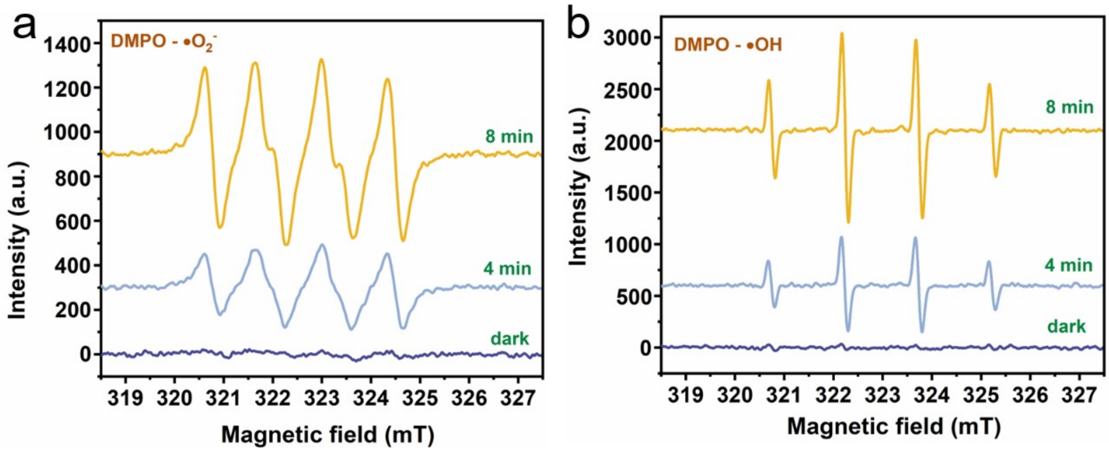

Figure S13. ESR spectra of DMPO-trapped ·O^{2-} and ·OH using In_2S_3@ZIF-8@$ZnIn_2S_4$ samples subjected to 4 and 8 min visible light irradiation.

Table S1 Data comparison of photocatalytic Cr(VI) reduction performance over different catalysts using 300 W Xenon lamp with 420 nm cut-off filter.

Catalysts	Catalysts quantity (50 mL of 20 mg L^{-1} Cr(VI) aqueous solution)	photocatalytic capacity	Reference
ZIF-8	50 mg	10% within 30 min	1
CZS@Z60	50 mg	100% within 10 min	1
MoO_3@ZIF-8	25 mg	96% within 40 min	2
$ZnIn_2S_4$	20 mg	75.1% within 120 min	3
CNFs/ $ZnIn_2S_4$	20 mg	100% within 60 min	3
In_2S_3	35 mg	75.9% within 6 min	4
Ti_3C_2@In_2S_3	35 mg	100% within 6 min	4
In_2S_3@ZIF-8@$ZnIn_2S_4$	**5 mg**	**97.8% within 30 min**	**This work**

REFERENCES

1. J. H. Qiu, X. F. Zhang, X. G. Zhang, Y. Feng, Y. X. Li, L. Y. Yang, H. Q. Lu and J. F. Yao, Constructing $Cd_{0.5}Zn_{0.5}S$@ZIF-8 nanocomposites through self-assembly strategy to enhance Cr(VI) photocatalytic reduction, *J. Hazard. Mater.*, 2018, **349**, 234-241.
2. Y. Zhang and S.-J. Park, Facile construction of MoO_3@ZIF-8 core-shell nanorods for efficient photoreduction of aqueous Cr (VI), *Applied Catalysis B: Environmental*, 2019, **240**, 92-101.
3. J. H. Qiu, M. Li, Y. Yang and J. F. Yao, Facile construction of three-dimensional netted $ZnIn_2S_4$ by cellulose nanofibrils for efficiently photocatalytic reduction of Cr(VI), *Chem. Eng. J.*, 2019, **375**.
4. H. S. Huang, X. Jiang, N. J. Li, D. Y. Chen, Q. F. Xu, H. Li, J. H. He and J. M. Lu, Noble-metal-free ultrathin MXene coupled with In_2S_3 nanoflakes for ultrafast photocatalytic reduction of hexavalent chromium, *Appl. Catal. B: Environ*, 2021, **284**.